Arctic/Atlantic Exchanges via the Subpolar Gyre*

HELENE R. LANGEHAUG

Nansen Environmental and Remote Sensing Center, and Bjerknes Centre for Climate Research, Bergen, Norway

ISELIN MEDHAUG AND TOR ELDEVIK

Geophysical Institute, University of Bergen, and Bjerknes Centre for Climate Research, Bergen, Norway

ODD HELGE OTTERÅ

Uni Bjerknes Centre, and Bjerknes Centre for Climate Research, Bergen, Norway

(Manuscript received 8 February 2011, in final form 7 October 2011)

ABSTRACT

In the present study the decadal variability in the strength and shape of the subpolar gyre (SPG) in a 600-yr preindustrial simulation using the Bergen Climate Model is investigated. The atmospheric influence on the SPG strength is reflected in the variability of Labrador Sea Water (LSW), which is largely controlled by the North Atlantic Oscillation, the first mode of the North Atlantic atmospheric variability. A combination of the amount of LSW, the overflows from the Nordic seas, and the second mode of atmospheric variability, the East Atlantic Pattern, explains 44% of the modeled decadal variability in the SPG strength. A prior increase in these components leads to an intensified SPG in the western subpolar region. Typically, an increase of one standard deviation (std dev) of the total overflow (1 std dev = 0.2 Sv; 1 Sv $\equiv 10^6$ m^3 s^{-1}) corresponds to an intensification of about one-half std dev of the SPG strength (1 std dev = 2 Sv). A similar response is found for an increase of one std dev in the amount of LSW, and simultaneously the strength of the North Atlantic Current increases by one-half std dev (1 std dev = 0.9 Sv).

1. Introduction

The subpolar North Atlantic Ocean (Fig. 1) is a region of complex dynamics, playing a key role in the variability of Earth's climate (Hátún et al. 2005; Schott and Brandt 2007; Lozier 2010). The cyclonic circulation of the subpolar gyre (SPG) is a dominant feature of the subpolar North Atlantic and constitutes an important part of the Atlantic meridional overturning circulation (AMOC; Kuhlbrodt et al. 2007). The variable SPG is maintained by buoyancy contrasts and overflows from neighboring seas, as well as by wind forcing. The northward-flowing eastern branch of the SPG (above 1000 m) includes the North Atlantic Current (NAC; Fig. 2), supplying the gyre with warm and saline water from the subtropics (McCartney and Talley 1982). In the western part of the SPG cold and fresh polar water (PW) is carried by the East Greenland Current (EGC) through the Denmark Strait (Aagaard and Carmack 1989). The southward export of sea ice and freshwater through the Canadian Archipelago is also feeding the SPG with cold freshwater (Tang et al. 2004; Curry et al. 2011).

In winter, the SPG is cooled through surface heat loss leading to deep convection and subsequent formation of Labrador Sea Water (LSW) in the Labrador Sea (Talley and McCartney 1982; Curry et al. 1998; Eden and Willebrand 2001). Another deep water component is formed in the Nordic seas. This component spills over the Greenland–Scotland Ridge (GSR) as cold and dense overflow water (OW) and flows into the Labrador Sea (Dickson and Brown 1994). The OW is a product of the densification of the Atlantic boundary current in the Arctic Mediterranean (comprising the Nordic seas and the Arctic Ocean; Mauritzen 1996; Rudels et al. 1999;

* Bjerknes Centre for Climate Research Publication Number A375.

Corresponding author address: H. R. Langehaug, Nansen Environmental and Remote Sensing Center, Thormøhlensgate 47, N-5006 Bergen, Norway.
E-mail: helene.langehaug@nersc.no

DOI: 10.1175/JCLI-D-11-00085.1

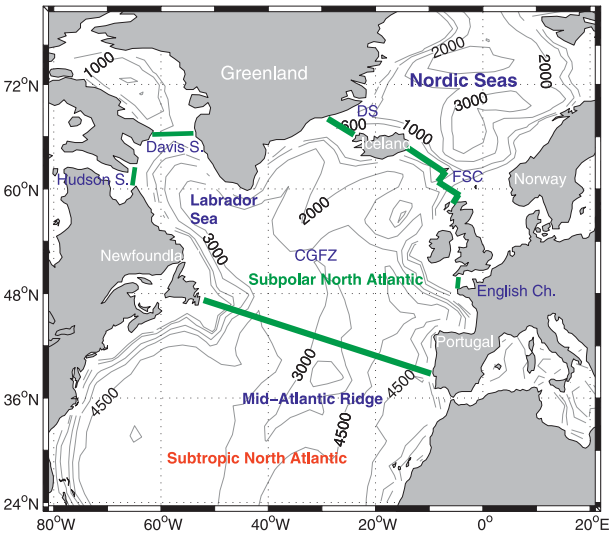

FIG. 1. The model bathymetry (depth in m) of the North Atlantic Ocean and Nordic seas, with names that are referred to in the text. Abbreviations: Denmark Strait (DS), Faroe–Shetland Channel (FSC), Charlie–Gibbs Fracture Zone (CGFZ). The green sections close the subpolar region.

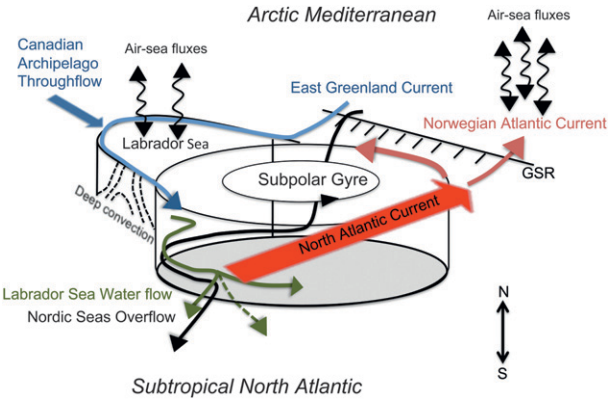

FIG. 2. Schematic of the main circulation in the subpolar North Atlantic.

Eldevik et al. 2009). At depths below 1000 m the circulation of OW and LSW dominates the SPG circulation (Fig. 2), where the LSW circulates above the OW. The deep western boundary current (DWBC; Smethie et al. 2000; Smethie and Fine 2001) is the major constituent of the lower limb of AMOC and carries OW and LSW through the northern North Atlantic to lower latitudes (Lumpkin and Speer 2003; Medhaug et al. 2012). The total volume transport of the DWBC is about 12.9 Sv ($1\ \text{Sv} \equiv 10^6\ \text{m}^3\ \text{s}^{-1}$) when measured east of the Grand Banks (Schott et al. 2004).

Several model studies have investigated the importance of the Nordic seas overflow on the SPG circulation (e.g., Böning et al. 1996; Redler and Böning 1997; Roberts and Wood 1997; Born et al. 2009). Redler and Böning (1997) identified the role of the overflow on the upper and lower circulation in the North Atlantic from a high-resolution ocean model. They concluded that the AMOC was mainly sensitive to the overflow rather than to the open-ocean convection process driven directly by air–sea fluxes over the subpolar region. From a coupled climate model sensitivity experiment, Born et al. (2009) found that the model's representation of the overflow had a large influence on the properties of the SPG and that a more vigorous overflow led to a strengthened SPG. Redler and Böning (1997) suggested that the overflow in the Denmark Strait is the main controlling mechanism for the DWBC, while changes in the flow through the Faroe Bank Channel have only a small effect on the deep transport in the western basin. Nevertheless, the magnitude and variability of the DWBC is still not well understood (Bacon and Saunders 2010; Lozier 2010). Although some model transport estimates have been compared with observations at the GSR, only a few model studies have investigated the downstream development of the DWBC (Bacon and Saunders 2010).

There are several known deficits in the representation of ocean circulation in climate models. For instance, these models are typically non-eddy-permitting and therefore do not resolve processes over small-scale topography, as well as small-scale boundary currents, very well (de Jong et al. 2009). In addition, overflow processes, such as mixing and entrainment of Atlantic Water (AW), are generally operating on subgrid scales and therefore need to be parameterized (Legg et al. 2009). These processes and the subsequent transformation of the overflow as it descends the GSR set the properties of the water masses constituting the deepest branch of the overturning circulation (Lauderdale et al. 2008; Cenedese and Adduce 2010). A realistic representation of the dense overflow from the Nordic seas is therefore important when assessing the relative contributions of the deep water formation in the Labrador Sea and Nordic seas to the circulation of the Atlantic Ocean (Döscher and Redler 1997; Bailey et al. 2005).

The hydrographic properties in the subpolar North Atlantic undergo pronounced variations on decadal-to-centennial time scales (Sarafanov 2009; van Aken et al. 2011), partly as a consequence of changes in the local atmospheric conditions associated with the winter North Atlantic Oscillation (NAO). For instance, a positive phase of the NAO is associated with strong heat loss in the Labrador Sea. In addition, the EGC and the associated coastal current are important sources of low-salinity water south of the Denmark Strait and play an important role in controlling the freshwater distribution in the western North Atlantic (Sutherland and Pickart 2008).

The inflow of low-salinity water masses from these currents, together with inflow of Subtropical Water (STW) from the east, are essential for the preconditioning of the deep convection and the following restratification of the water column in the Labrador Sea (Marshall and Schott 1999; Hátún et al. 2007). It is a challenge, however, to realistically simulate temperature and salinity in the Labrador Sea, since climate models are non-eddy-resolving and, hence, keep the interior Labrador Sea generally too saline (Bailey et al. 2005). This challenge is apparently not limited to climate models, as it has also been demonstrated in a comparison study using regional eddy-resolving models (Tréguier et al. 2005).

Furthermore, there are also processes in the atmosphere that are not resolved in coarse-resolution climate models, such as barrier winds and tip jets in the vicinity of Cape Farwell (Moore and Renfrew 2005). The Greenland tip jet leads to increased heat loss and wind stress in the Irminger Sea, which can enhance deep convection in this region (Pickart et al. 2003). Since this tip jet is unresolved, this would likely lead to an underestimation of the amount of deep water produced in the Labrador and Irminger seas and thus affect the variability of dense water formation in these regions. Hence, in a recent study, Sproson et al. (2010) present an approach to parameterize the Greenland tip jet in climate models. However, such a parameterization has generally not been implemented in most climate models, so its effect on ocean circulation in models is so far uncertain.

Fully coupled climate models are valuable tools for investigating the SPG and the mechanisms controlling its variability on decadal to multidecadal time scales (Delworth and Mann 2000; Cooper and Gordon 2002; Gao and Yu 2008; Born et al. 2009). In general, climate variability on time scales longer than a few decades cannot be investigated directly from observations because of the limited length of continuous time series. Model studies focusing on the subpolar North Atlantic have so far mostly been restricted to hindcast simulations with ocean general circulation models (OGCMs) forced with atmospheric reanalysis fields (Hátún et al. 2005; Böning et al. 2006; Deshayes and Frankignoul 2008; Lohmann et al. 2009). The proposed mechanisms in OGCM studies should thus be tested in coupled climate models to establish to what degree such mechanisms are robust among different models and at different time scales (Gao and Yu 2008).

The main objective of this study is to identify key components that contribute to decadal-scale variability in the strength of the SPG as manifested in a multicentury climate model simulation. In particular, the influence of decadal variations in the different currents flowing into and out of the subpolar region on the SPG is assessed, with a special emphasis on the deep branches and their pathways within the subpolar region. For this study, a 600-yr control simulation with the Bergen Climate Model (BCM; Otterå et al. 2009) has been used. One advantage of using such a long model integration is the possibility of studying mechanisms and natural climate variability on decadal to multidecadal time scales.

The paper is organized as follows. The model, observations, and the methods used are presented in section 2. The model performance in the subpolar region is described in section 3, where the key sections constraining the subpolar region are assessed. Different components controlling the SPG strength are then identified and combined in order to explain the decadal-scale variability in SPG strength. Finally, a discussion and a summary are given in sections 4 and 5, respectively.

2. Data and methods

a. Model description

The model run used in this study is a 600-yr-long simulation of the preindustrial climate with the BCM, a fully coupled atmosphere–ocean–sea ice general circulation model. A general description of the model can be found in Furevik et al. (2003), with further information about this version and simulation given in Otterå et al. (2009). The same version was used in Otterå et al. (2010), but their study also includes the effect of volcanoes and solar variability. The BCM consists of the Miami Isopycnic Coordinate Ocean Model (MICOM; Bleck et al. 1992) coupled with the atmospheric model Action de Recherche Petite Echelle Grande Echelle/Integrated Forecast System (ARPEGE/IFS; Déqué et al. 1994) and a dynamic–thermodynamic sea ice model (GELATO; Salas-Mélia 2002).

MICOM has been modified in a number of ways since the original version (Otterå et al. 2009, 2010). The present version of MICOM uses potential density with reference pressure at 2000 dbar as vertical coordinate (σ_2 coordinate), whereas the previous version of BCM used 0 dbar as reference pressure (σ_0 coordinate). As a consequence, the new version of MICOM shows a more pronounced deep circulation cell of Antarctic Bottom Water extending into the Atlantic (Otterå et al. 2009). The diapycnal mixing is a function of background diffusivity dependent on the local stability (McDougall and Dewar 1998), and to incorporate shear instability and gravity current mixing, a Richardson number–dependent diffusivity has been added (Orre et al. 2010). The latter development greatly improves the water mass characteristics downstream of overflow regions.

The horizontal ocean grid is almost regular, with a spacing of approximately 2.4° latitude × 2.4° longitude.

To better resolve tropically confined dynamics the latitudinal grid spacing is gradually reduced to 0.8° near the equator. The ocean model consists of 34 isopycnic layers, ranging from 1030.119 to 1037.800 kg m^{-3}, below a nonisopycnic mixed layer. ARPEGE is run with a truncation at wavenumber T_L63 on a reduced Gaussian grid, indicating a spatial resolution of approximately 2.8° along the equator and a total of 31 vertical levels, ranging from the surface to 20 hPa.

The initial conditions for the preindustrial integration are obtained from the end of a 500-yr spinup (Otterå et al. 2009). During the first spinup phase the ocean–sea ice component of the coupled model was run alone for 100 yr starting from observed climatology (Steele et al. 2001) and with the ocean initially at rest. During this 100-yr integration, the ocean model was forced with two consecutive cycles of daily National Centers for Environmental Prediction/National Center for Atmospheric Research (NCEP/NCAR) reanalysis fields (Kalnay et al. 1996). The coupled system was then initialized with the final state of this ocean–sea ice spinup and then run in coupled mode for an additional 200 yr with constant, present-day (A.D. 2000) radiative forcing. Following the method outlined in Stouffer et al. (2004), the radiative forcing conditions were then gradually changed to preindustrial (A.D. 1850) values over a period of 50 yr and then kept constant thereafter. In the final spinup phase the coupled model was run for another 150 yr to allow the simulated climate to adjust, at least partially, to the preindustrial regime. The model is run without any form of flux adjustments and is thus free to evolve its own climate.

b. Study area and statistical methods

The subpolar region is closed by five sections (Fig. 1): Newfoundland–Portugal (hereafter referred to as the Newfoundland section), English Channel, GSR, Davis Strait, and Hudson Strait. In the present study, the SPG strength is defined as the absolute value of the minimum barotropic streamfunction in the subpolar region, a measure that is commonly used within the modeling community (Eden and Willebrand 2001; Tréguier et al. 2005; Lohmann et al. 2009). The NAO (Barnston and Livezey 1987; Hurrell 1995) and the East Atlantic Pattern (EAP; Barnston and Livezey 1987) are represented by the first and second empirical orthogonal functions (EOFs) of the mean winter sea level pressure (November–April) within 20°–80°N and 90°W–40°E, respectively, in line with previous studies (Wanner et al. 2001; Häkkinen and Rhines 2004; Medhaug et al. 2012). The indices are given by the corresponding principal components.

To filter out high-frequency variability, all time series have been low-pass filtered using an 11-yr running Bartlett window. In the correlation/regression analysis the time series are also linearly detrended. A standard Student's t test has been used to calculate the significance. Autocorrelation has been taken into account by adjusting the effective number of degrees of freedom following the method of Chelton (1983). All correlations given in the text are significant above the 95% confidence level. Furthermore, a composite analysis has been used to show relationships at different climatic states (Brauch and Gerdes 2005; Lohmann et al. 2009). The composites have been obtained from values associated with large values for specific variables, that is, years when the variables are larger than 1.5 standard deviations (std dev) of the filtered time series. A similar criterion was also used in Thompson and Wallace (2001). A t test is performed with the null hypothesis being that the composites and the average of all years have the same mean value. When this null hypothesis can be rejected, the composites are significant above 95% confidence level.

c. Observations

To assess the model performance we have applied hydrographic data from the Norwegian Iceland Seas Experiment (NISE; Nilsen et al. 2008) and the World Ocean Circulation Experiment (WOCE; Schlitzer 2000) datasets. The NISE dataset comprises the northern North Atlantic, the Nordic seas, and the Barents Sea for the time period 1900–2006. Here we have used data at the GSR for the time period 1950–2005, which covers the period when the majority of the NISE data was collected. We do not expect this dataset to be biased by a specific type of forcing, since this period contains both relatively warm and cold phases of ocean climate (Curry and McCartney 2001; Eldevik et al. 2009). The global WOCE dataset was sampled in the decade from 1988 until 1998. From the late 1980s to the mid-1990s there was an intense deep convection in the Labrador Sea, producing the densest and deepest LSW on record (Lazier et al. 2002; Yashayaev 2007). This time period corresponded to a positive phase of both the NAO (Dickson et al. 1996) and the EAP (http://www.cpc.ncep.noaa.gov/). We have used WOCE data from a section stretching from Newfoundland to Portugal, and the resulting LSW found in this section is therefore likely biased toward higher than average densities.

3. Results

a. Model performance in the subpolar region

The performance of the BCM in the subpolar North Atlantic is assessed because this region poses a particular challenge for ocean models because of its complex hydrography and ocean circulation (Zhu et al. 2010).

Here the GSR and Newfoundland sections are of prime focus, since these sections capture the dominant water masses flowing into and out of the subpolar region (Fig. 1). The mean model temperature and salinity in these sections are compared with observed hydrography.

The mean barotropic streamfunction and mean mixed layer velocity in the North Atlantic are shown in Fig. 3. Both the subpolar and the subtropical gyres are evident, with their cyclonic (negative) and anticyclonic (positive) circulations, respectively. The NAC is situated at the border between the two gyres. The SPG has three great arms: one extending toward the Faroe Islands, one toward the Denmark Strait, and the last toward the Davis Strait. The mean barotropic streamfunction has a minimum south of Cape Farewell, with an average strength of −30 Sv. This compares well with observed estimates that range from −40 to −25 Sv (Clarke 1984; Bacon 1997).

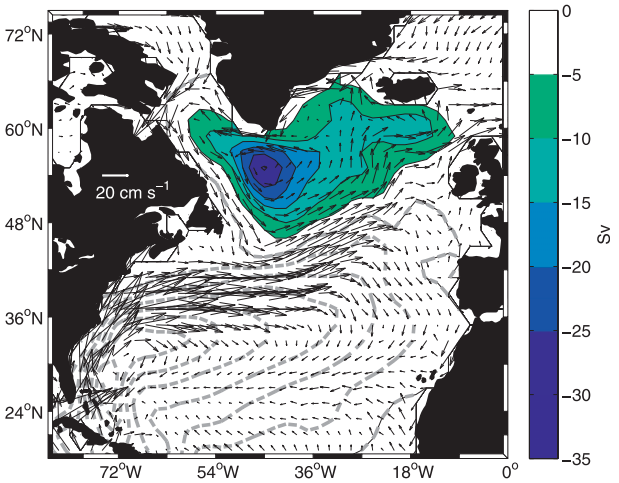

FIG. 3. Mean barotropic streamfunction (contours) of the North Atlantic Ocean, where the subpolar gyre is highlighted with color. The streamfunction is given with 5-Sv intervals, where filled contours indicate negative values and dashed lines indicate positive values. Mean mixed layer velocities are shown by black arrows, with a reference velocity of 20 cm s^{-1}.

1) NEWFOUNDLAND SECTION

The WOCE data (Figs. 4a,c) show a fresh layer on the western continental slope in the upper 500 m and a distinct warm and saline Atlantic layer in the upper 1000 m. The core of the NAC, characterized by salinities up to 36.25, is located west of the Mid-Atlantic Ridge (~40°W). A colder and fresher intermediate layer (1500–2500 m) is also present west of the ridge, with the coldest and freshest deep water found below this layer. On the eastern side of the ridge, between the intermediate layer and the deepest water at 2500–3500 m, there is a layer of relatively high salinity.

The spatial structure of the model temperature and salinity in the Newfoundland section compares well with the observations, except for the deep eastern part (Figs. 4b,d), where the simulated deep water is too warm and saline. The temperatures and salinities below ~1000 m are in general higher than in the observations. Another distinct difference between the simulated and the observed sections is the location of the core of the northward-flowing NAC. The observed NAC curves around Grand Banks before it detaches from the American coastline (Schott and Brandt 2007), while the simulated NAC detaches farther south (Fig. 3). This difference can be seen as an eastward shift of the simulated NAC in the Newfoundland section compared to the observations. This shift is probably caused by too zonal westerly winds in the northern North Atlantic, leading to a more zonally oriented NAC (Otterå et al. 2009).

The baroclinic velocity field with zero-velocity reference at 1600 m has been calculated from the observed and modeled hydrograhpy (not shown). These calculations confirm the hydrographic similarities and discrepancies identified above. The velocity fields are comparable in the eastern- and westernmost part of the Newfoundland section, whereas relatively large differences appear close to the Mid-Atlantic Ridge. This is also where the location of the model section and the WOCE section differs the most. Overall, the model velocities are weaker than the observation-based estimates. This is mostly due to the weak gradients found in the model hydrography compared to the observations.

Five water masses are defined in the model Newfoundland section (see Fig. 4b for location): STW, LSW, Mediterranean Water (MW), Iceland–Scotland overflow water (ISOW), and Denmark Strait overflow water (DSOW). These water masses are defined by using σ_2, salinity, and potential temperature criteria (Table 1). The mean transports of the associated currents are given in Table 2. The mean model NAC is 26.0 Sv, while the observed NAC has been estimated to 21 Sv (Pèrez-Brunius et al. 2004). The simulated transport of DSOW is on average 3.9 Sv, which is in good agreement with the observation-based estimates of 3.8–4.6 Sv (Schott et al. 2004; Dengler et al. 2006). The southward model transport of ISOW is 3.8 Sv. The transport of LSW from observation-based estimates decreases considerably from north (11.3 Sv) to south (3.3 Sv) of Grand Banks (Schott et al. 2004; Dengler et al. 2006), with the model transport of 4.9 Sv falling well within this range. The temperature and salinity of the different water masses vary on interannual and (multi)decadal time scales (not shown). However, since the respective time series are not found to have a significant correlation with the SPG strength, the hydrographic variability is not considered further.

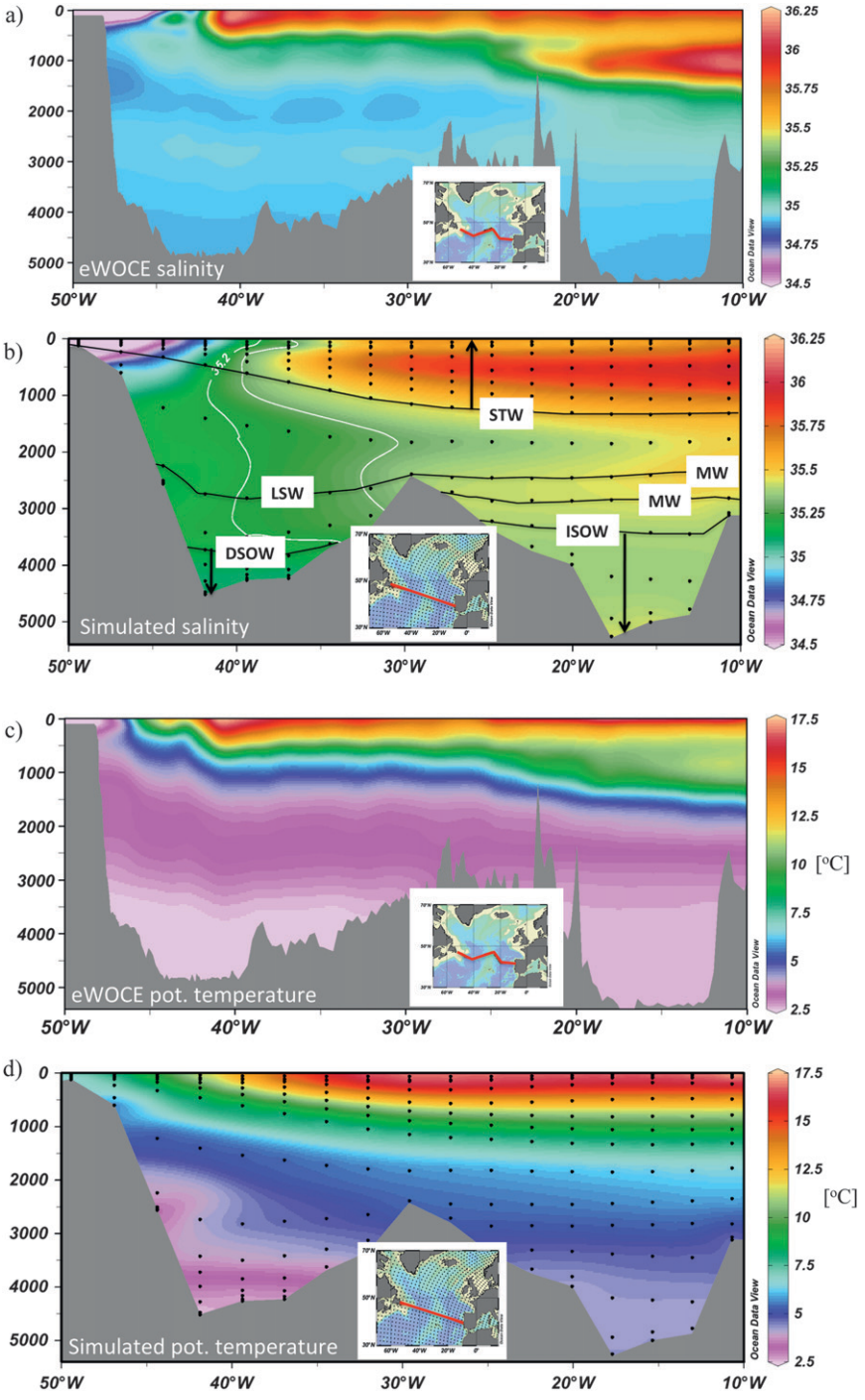

FIG. 4. Salinity and potential temperature (°C) in the Newfoundland section from (a),(c) the WOCE data and for (b),(d) the Bergen Climate Model. Black dots show the center of the grid cells. The locations of the water masses Subtropical Water (STW), Labrador Sea Water (LSW), Mediterranean Water (MW), Denmark Strait overflow water (DSOW), and Iceland–Scotland overflow water (ISOW) are indicated. Note the slight difference in the locations of the observed and modeled sections.

TABLE 1. Definitions of the water masses in the various sections by using σ_2 isopycnals (the vertical level of BCM), salinity (S), and potential temperature (T) criteria. The mixed layer (ML) is a nonisopycnic layer.

Water mass	Abbreviation	Layers, σ_2 (kg m^{-3})	S/T limit
Subtropical Water	STW	$\sigma_{2,\mathrm{ML}}$–$\sigma_{2,15}$ (=36.712)	
Labrador Sea Water	LSW	$\sigma_{2,17}$ (=36.946)	$S < 35.3$
Mediterranean Water	MW	$\sigma_{2,17}$–$\sigma_{2,18}$ (=37.020)	$S \geq 35.3$
Denmark Strait overflow water	DSOW	$\sigma_{2,19}$ (=37.074)–$\sigma_{2,35}$	$S < 35.2$
Iceland–Scotland overflow water	ISOW	$\sigma_{2,19}$ (=37.074)–$\sigma_{2,35}$	$S \geq 35.2$
Atlantic Water	AW	$\sigma_{2,\mathrm{ML}}$–$\sigma_{2,16}$ (=36.846)	$S > 34.7$; $T > 8$°C
Polar Water	PW	$\sigma_{2,\mathrm{ML}}$–$\sigma_{2,16}$ (=36.846)	$S \leq 34.7$; $T \leq 8$°C
Overflow water	OW	$\sigma_{2,17}$–$\sigma_{2,35}$ (=37.800)	

To identify the pathways of DSOW and ISOW in the subpolar region, the fraction of these water masses in the water column has been calculated. The DSOW is found to occupy the deep western North Atlantic basin (Fig. 5, top), while the ISOW occupies the eastern part (Fig. 5, bottom). A salinity criterion (35.2) is used to separate the two overflows south of the GSR, while north of the GSR there is a common source for the two overflows with a salinity lower than 35.2. From the mean velocity of the deep layers, the DSOW and ISOW appear to originate from the Denmark Strait and Faroe–Shetland Channel, respectively. An additional salinity criterion (38.0) is added to ISOW to exclude the fraction of very saline water masses from the Mediterranean Sea (Fig. 5).

The ISOW is observed to flow through the Charlie–Gibbs Fracture Zone (CGFZ; see Fig. 1; Dickson and Brown 1994; Schott et al. 1999; Smethie and Fine 2001; LeBel et al. 2008) and around the Reykjanes Ridge into the Irminger Basin. It then becomes part of the DWBC, sandwiched between the LSW and the DSOW (Yashayaev 2007). In BCM there is no ISOW flowing through the CGFZ. Hence the ISOW has to flow southward in the eastern part of the North Atlantic basin or recirculate back north. The flow through the CGFZ is difficult to simulate because of two factors: 1) the smoothing of the bathymetry in the coarse-resolution model, and 2) the depth of the isopycnals in the model may be different from the real world. Consequently, a shallow model CGFZ together with a deep position of the model isopycnals could act as a barrier for deep flow through the CGFZ.

TABLE 2. Long-term mean volume transport (flux) for the currents flowing across the Newfoundland section and the Greenland–Scotland Ridge. The sections are aligned approximately east–west, and the flow direction is therefore given in the following manner: positive is northward and negative is southward. The volume transport for each current is constrained by the definition of the associated water mass (Table 1). Net flow is calculated for the currents at the GSR, to take into account recirculating water, while southward or northward flow is used at the Newfoundland section.

Current	Abbreviation	Flux (Sv)	Water mass
North Atlantic Current	NAC	26.0	STW
Labrador Sea Water flow	LSW flow	−4.9	LSW
Mediterranean Water flow	MW flow	−3.9	MW
Denmark Strait overflow	DS overflow	−3.9	DSOW
Iceland–Scotland overflow	IS overflow	−3.8	ISOW
Norwegian Atlantic Current	NwAC	7.4	AW
East Greenland Current	EGC	−2.1	PW
Overflow	Overflow	−5.7	OW

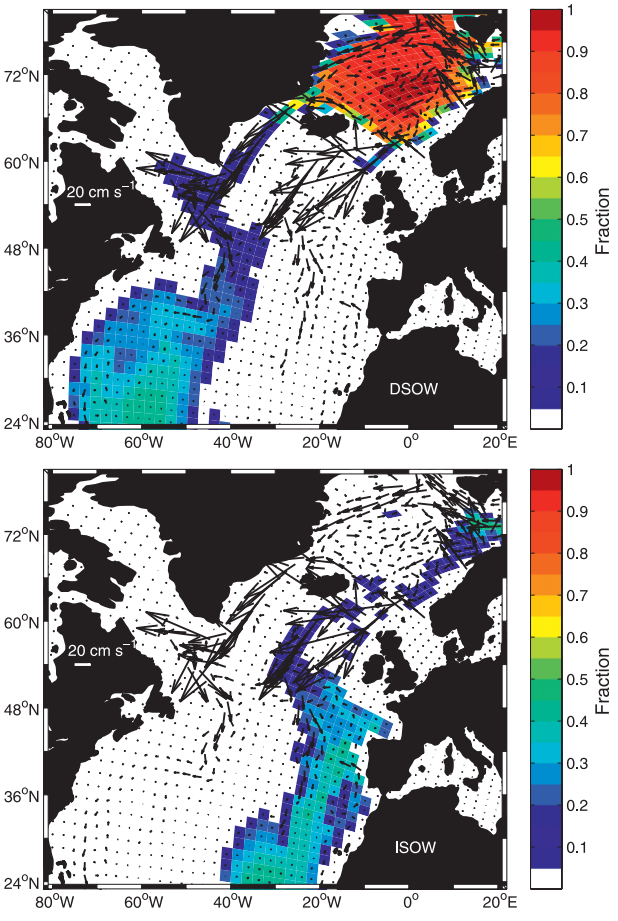

FIG. 5. Deep water velocities (layers 19–35; arrows) and fraction of the total water column (color) consisting of (top) DSOW and (bottom) ISOW. The reference velocity is 20 cm s^{-1}.

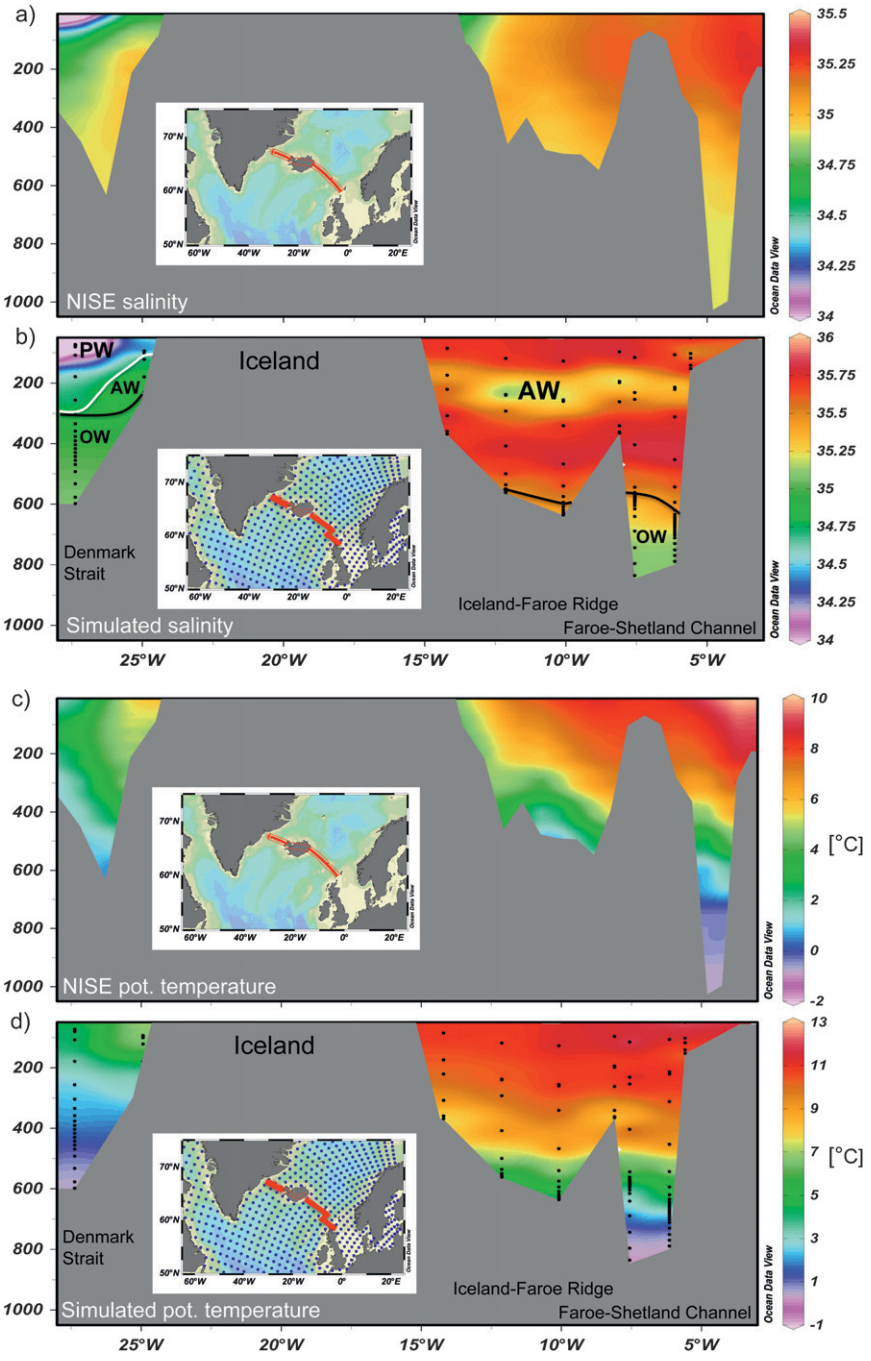

FIG. 6. Salinity and potential temperature (°C) at the Greenland–Scotland Ridge from (a),(c) the NISE data and for (b),(d) the Bergen Climate Model. Black dots show the center of the grid cells. The locations of the water masses Atlantic Water (AW), Polar Water (PW), and overflow water (OW) are indicated. To emphasize similarities and dissimilarities in the structure of the respective fields, note that the temperature and salinity ranges are different between the observations and the model. This difference can be seen in Fig. 7.

2) GREENLAND–SCOTLAND RIDGE

The NISE data (Figs. 6a,c) show warm and saline water masses in the eastern Denmark Strait and in the upper 500 m between Iceland and Shetland. A fresh layer is found in the upper 100 m in the western Denmark Strait. Below 400 m, the water is relatively saline and generally colder than 2°C. The spatial structure of the model

temperature and salinity in the GSR section (Figs. 6b,d) compare well with the observations, especially regarding the temperature. The comparison of the salinity reveals some differences, such as a fresher intermediate layer between Iceland and Shetland, and a weaker gradient between the eastern and western Denmark Strait in the model.

Three water masses are defined at the model GSR (see Fig. 6b for location): AW, Polar Water (PW), and OW. These water masses are defined by using σ_2, salinity, and potential temperature criteria (Table 1). A salinity limit (34.7) is applied to distinguish between the PW and AW in the Denmark Strait. By using this limit, most of the water that moves northward in the Denmark Strait is labeled AW. This flow is the model representation of the Irminger Current. In observation-based studies the Irminger Current is found to carry salinities above 34.8 (Holliday et al. 2006).

The water masses found at the GSR have more distinctly separated temperature and salinity properties compared to the water masses in the Newfoundland section. Therefore, the water mass exchange across the GSR is visualized using a volumetric temperature and salinity (T–S) diagram (Fig. 7), the traditional way of classifying water masses in observational studies. Three water masses stand out in this analysis: the warm and saline AW, the cold and fresh PW, and the cold and dense OW. The rather distinct partition of these three components in the coarse-resolution BCM is surprising with respect to what is seen in other coupled climate models (de Jong et al. 2009). The water mass transformation in the Nordic seas, reflected in these three branches, is discussed in more detail in Medhaug et al. (2012). The thermohaline contrasts spanned by the three water masses are similar to the observed, but the model hydrography is skewed toward warmer and more saline properties, especially for the AW and PW.

The volume transports of AW, PW, and OW across the GSR are the Norwegian Atlantic Current (NwAC), the EGC, and the overflow, respectively (Table 2). The NwAC is found to be 8.5 Sv (Østerhus et al. 2005), while the average model transport is 7.4 Sv. The mean model EGC is 2.1 Sv, while the observational estimates are typically found to lie between 0.4 and 2.1 Sv (Nilsson et al. 2008). The observation-based estimate of the total overflow is 6.4 Sv (Olsen et al. 2008) and is in reasonable agreement with the simulated value of 5.7 Sv. The distribution of the model overflow east and west of Iceland is 3.8 and 1.9 Sv, respectively, with the overflow between Iceland and the Faroe Islands being negligible. Observations suggest that the overflow should be about equally distributed with 3 Sv both east and west of Iceland (Olsen et al. 2008). It should be noted, however, that a realistic flow over narrow ocean passages, such as the Denmark Strait and the Faroe–Shetland Channel, is difficult to achieve in coarse-resolution models since the grid size does not allow the model to properly resolve the small-scale topographic features. Consequently it is also difficult to simulate the correct geographical distribution of the overflow.

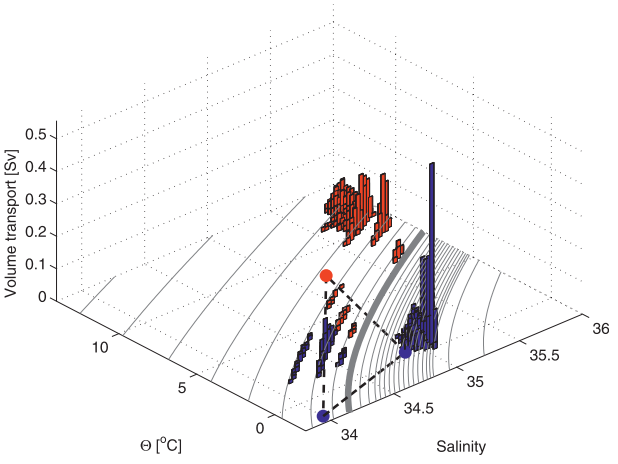

FIG. 7. Volumetric T–S diagram for the Greenland–Scotland Ridge. Red (blue) bars denote net northward (southward) volume transport larger than 0.01 Sv within the corresponding T–S interval. The dashed triangle shows the observed properties of Atlantic Water (AW), Polar Water (PW), and overflow water (OW) (Rudels et al. 1999; Eldevik et al. 2009). The σ_2 isolines illustrate the vertical discretization of the model, where the thick gray line is the upper isopycnal (layer 17) defining the OW. The properties of the mixed layer are seen as a continuous distribution of squares for the AW.

To estimate the time scales associated with the southward propagation of the overflows, cross-correlations have been calculated between the overflows at the GSR and their counterpart at the Newfoundland section. The overflow in the Denmark Strait and the corresponding flow in the Newfoundland section (DS overflow) have a correlation of 0.6 at a 3-yr lag, where the former is leading. The time scale associated with the southward propagation of the overflow from the Faroe–Shetland Channel to the Newfoundland section (IS overflow) is similar to the one associated with the propagation of the overflow from the Denmark Strait. The correlation is, however, substantially lower ($r = 0.28$).

b. *Processes governing the decadal subpolar gyre strength*

To identify key processes affecting the decadal variability of the SPG strength, the relationship between the SPG strength and the flow of the water masses has been investigated. There is a strong relationship between the SPG strength and the overflow in the Denmark Strait ($r = 0.62$), where the overflow leads by 1 yr. However,

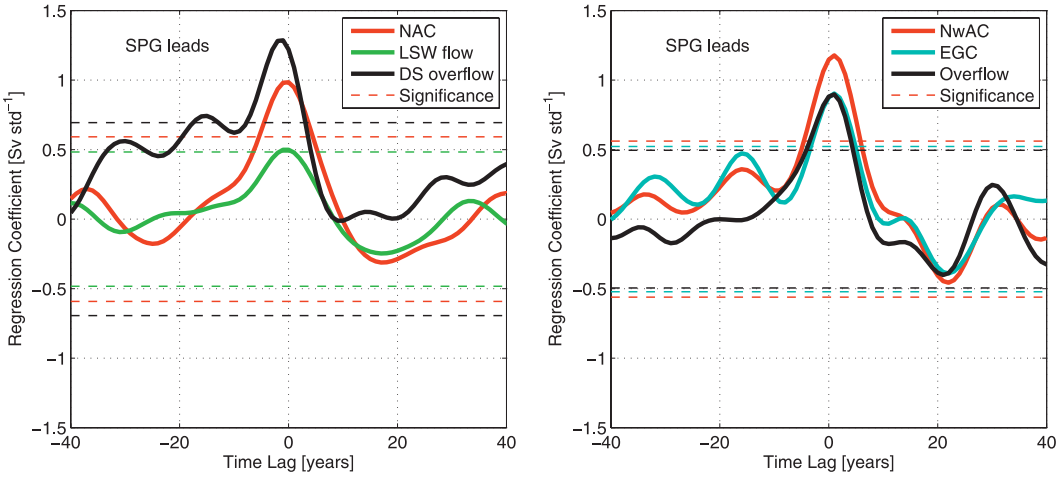

FIG. 8. SPG strength regressed on to the strength of the different flows across the (left) Newfoundland section and (right) Greenland–Scotland Ridge. An increase of one std dev for the DS overflow is associated with an enhancement of the SPG strength of 1.3 Sv, which is more than one-half std dev of the SPG strength (1 std dev = 2 Sv). Abbreviations are given in Table 2.

the SPG strength is anticorrelated with the overflow in the Faroe–Shetland Channel ($r = -0.49$, where the overflow leads by 2 yr). Unfortunately, there are no long-term observational records of the overflows (Olsen et al. 2008), but previous studies using regional ocean models suggest a dominant role for the overflow in the Denmark Strait both on the SPG and the total overflow (Redler and Böning 1997; Köhl et al. 2007). The latter also holds for BCM, where the correlation between the overflow in the Denmark Strait and the total overflow across the GSR is 0.82. Even though the overflow in the Faroe–Shetland Channel is about twice as large as the overflow across the Denmark Strait, the variability in the latter (1 std dev = 0.44 Sv) is larger than that of the overflow in the Faroe–Shetland Channel (0.31 Sv).

The SPG strength increases when the volume transports across the GSR and at the southern exit of the Labrador Sea increase (Fig. 8, with peak correlations in Table 3a). In the model, an increase of 1 std dev for the DS overflow (1 std dev = 0.7 Sv) is associated with an enhancement of the SPG strength of 1.3 Sv, which is more than half a std dev of the SPG strength (1 std dev = 2 Sv). This suggests that the variations in the DS overflow are instrumental for explaining the variability of the SPG strength. There is also a significant correlation between the IS overflow and the SPG strength, but with a time lag of 11 yr (Table 3). The northward-flowing warm and saline currents, NAC and NwAC, are also significantly correlated with the SPG strength (Fig. 8). The NwAC reflects changes in the overflow at the GSR. This is due to continuity since the exchanges across GSR are balanced to the first order. The correlation between the LSW flow at the Newfoundland section and the SPG strength is significant, but low (Fig. 8). On the other hand, there is a strong relationship between the latter and the formation of LSW in the Labrador Sea. This relationship will be addressed in the following subsection.

TABLE 3. Peak correlations (r) between the (a) subpolar gyre strength and (b) LSW thickness and the variables given in the table. Time series are low-pass filtered. Subpolar gyre strength/Labrador Sea Water thickness lags for negative lags (in yr). The wind stress is averaged both over the SPG region and over the Labrador Sea (LS), and the heat and freshwater fluxes over the LS.

(a) Subpolar gyre strength

Variables	r	Lag
NAC	0.35	+1
LSW flow	0.24	0
DS overflow	0.62	+1
IS overflow*	0.39	+11
NwAC	0.57	−1
EGC	0.43	−1
Overflow	0.43	−1
Sea surface height	0.70	−1
SPG wind stress	0.36	−6
EAP index	0.42	−5

(b) LSW thickness

Variables	r	Lag
SPG strength	0.47	0
Heat flux	0.41	−2
Freshwater flux	0.27	−2
LS wind stress	0.33	−1
NAO index	0.59	−1

* The time series of the IS overflow contains a nonlinear trend. Time scales shorter than 11 yr and longer than 100 yr have therefore been removed from the time series using a centered third-order Butterworth filter.

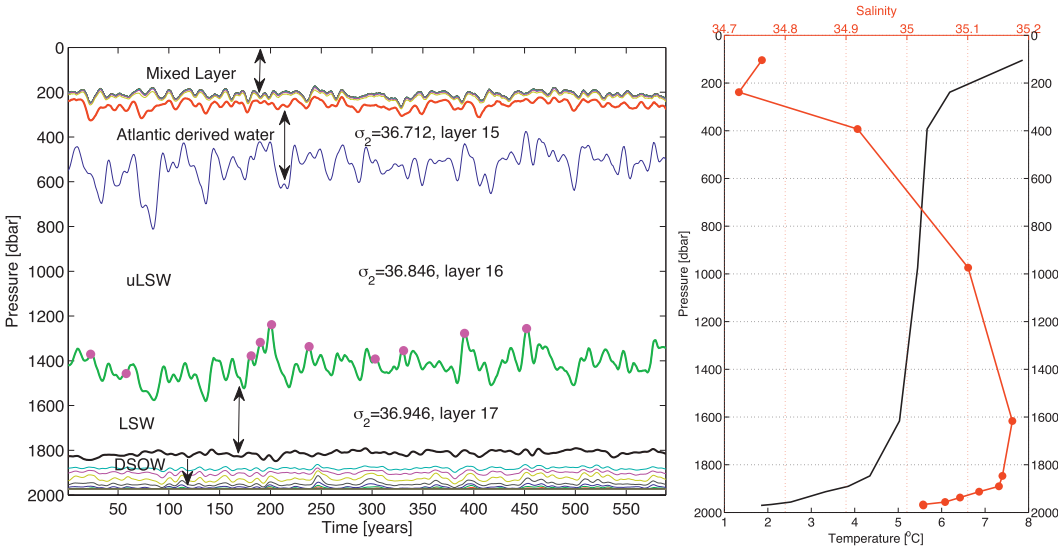

FIG. 9. (left) Time series for the depth of the layer interfaces (dbar) averaged over the Labrador Sea and (right) averaged temperature and salinity profiles in the Labrador Sea. Only layers thicker than 3 m are included in the profiles. Black arrows indicate layer thickness. The magenta dots show the end of NAO+ periods larger than 1.5 std dev of the filtered time series. The locations of the water masses upper Labrador Sea Water (uLSW), Labrador Sea Water (LSW), and Denmark Strait overflow water (DSOW) are indicated.

1) STRUCTURE OF THE LABRADOR SEA AND ATMOSPHERIC FORCING

Changes in the sea ice extent and sea ice thickness in the Arctic Mediterranean influence the freshwater input to the North Atlantic Ocean (Aagaard and Carmack 1989). Both the Davis Strait and Denmark Strait feed the Labrador Sea with freshwater from the Arctic Mediterranean. In this simulation the freshwater input to the Labrador Sea is most likely underestimated. This is likely due to the small sea ice extent in the vicinity of the Davis Strait compared to observations and also a generally too thin sea ice in the Arctic Mediterranean (Otterå et al. 2009). In addition, the lack of eddies in BCM keep the interior Labrador Sea more isolated from freshwater carried by the boundary currents.

To get a picture of the vertical structure in the Labrador Sea and, hence, the depth and range of the LSW, the average water column in the Labrador Sea is shown in Fig. 9. Layers 1, 14, and 15 have almost the same variability in thickness, temperature, and salinity, where layer 1 is the mixed layer, and layers 14 and 15 are Atlantic-derived water (layers 2 –13 are empty). Beneath these layers, there is a thick layer (layer 16). This layer is partly formed by deep convection in the Irminger Sea and at the northern rim of the Labrador Sea, ultimately as a result of gradual cooling of the STW. Eventually, this water mixes with the southward-flowing fresh Arctic waters in the Labrador and Irminger Seas. The resulting water mass will in the following be called upper LSW (uLSW). Another study indicates that the BCM is able to simulate the densification of STW in the eastern subpolar region well compared to observations (Langehaug et al. 2011, unpublished manuscript). The water in the layer below (layer 17) is named LSW, since this layer is mainly formed by deep convection in the Labrador Sea. The deepest water in the Labrador Sea mainly originates from the Denmark Strait (Fig. 5) and is therefore denoted DSOW in Fig. 9. The variability of the thickness of DSOW in the Labrador Sea has a correlation of 0.68 with the overflow in the Denmark Strait, where the latter leads by 1 yr. The temperature and salinity profiles (Fig. 9) show a warm and saline mixed layer, with fresh and relatively warm layers beneath. One can also note the very week stratification associated with the uLSW and LSW. The bottom layer contains cold and relatively fresh DSOW.

When the SPG strength increases there is an increased thickness in both layer 16 in the Irminger Sea and layer 17 in the Labrador Sea (Fig. 10), indicating the regions of uLSW and LSW formation, respectively. In the Labrador Sea the thickness of the uLSW and the LSW are anticorrelated; that is, when the SPG strength increases there is an associated increase in the thickness of the LSW and a subsequent decrease in the thickness of the uLSW. In the following we focus on the variability of LSW, since this water mass is the dominant product of the deep convection in the subpolar region for this simulation.

The atmospheric contribution to oceanic variability in the subpolar region is represented by fluctuations in

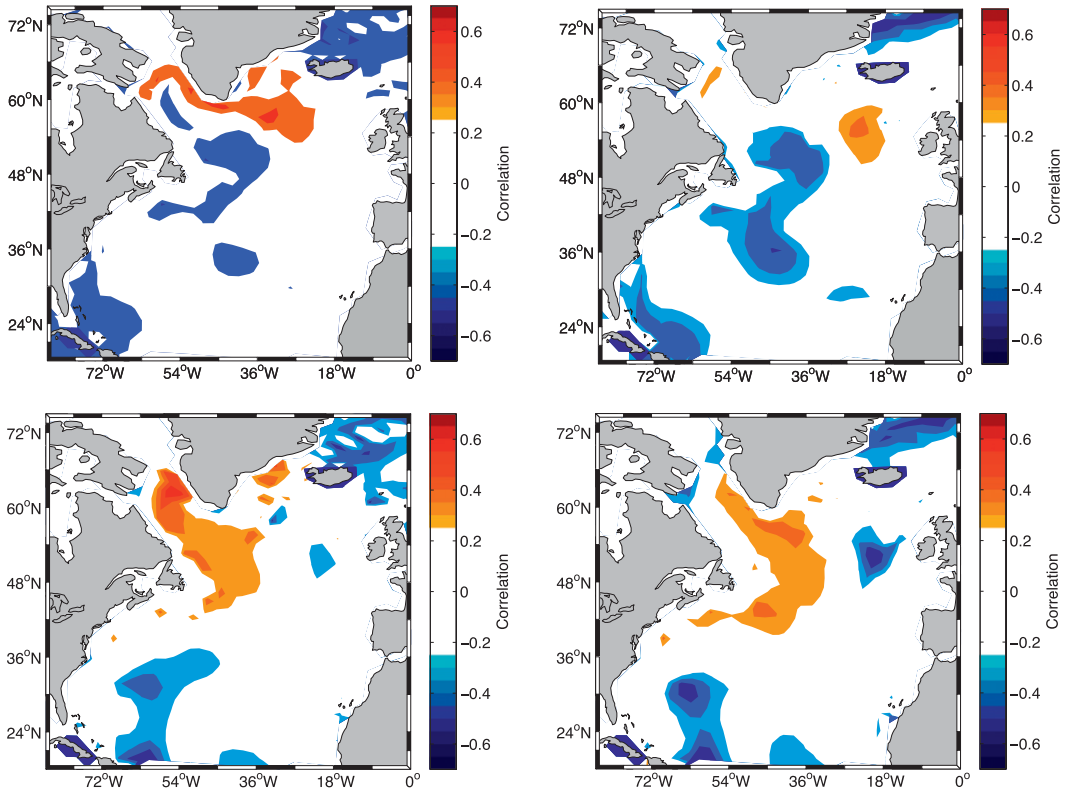

FIG. 10. Correlation between SPG strength and anomalies in the thickness of (top) layer 16 and (bottom) layer 17 at (left) SPG maximum and (right) 5 yr after SPG maximum.

the NAO and the EAP (Fig. 11). A positive NAO phase (NAO+) is associated with increased heat loss, less freshwater input, and stronger winds in the Labrador Sea (Medhaug et al. 2012), ultimately leading to an increased LSW thickness (Table 3b). Several previous studies have also suggested that there is a strong link between heat loss and deep water formation in the Labrador Sea (Curry et al. 1998; Yashayaev 2007; van Aken et al. 2011). The relationship between the LSW thickness and the NAO is indicated in Fig. 9, where the end of high NAO+ phases is marked in the figure. Even though the NAO is strongly related to the LSW thickness (Table 3b), the NAO does not have a significant correlation with the SPG strength. The EAP, on the other hand, has a significant correlation of 0.42 with the SPG strength (Table 3a). In particular, the EAP is strongly related to the wind stress in the subpolar region, with a correlation of 0.68 (wind stress leads by 1 yr).

2) INFLUENCE OF DEEP WATER

The present study, as well as previous studies (Redler and Böning 1997; Curry et al. 1998; Born et al. 2009), suggests that the SPG strength is strongly related to both the Nordic seas overflow and the deep water formation in the Labrador Sea. Here we explore these relationships further by investigating anomalies in the spatial extent of the SPG associated with increased overflow and LSW thickness, respectively. For this we have made composites of anomalies in the barotropic streamfunction following two different criteria (Fig. 12): 1) by only taking into account years with strong overflow, and 2) by only taking into account years with large LSW thickness. For a strong overflow (44 yr included in the composite), the central SPG intensifies by up to 2 Sv. A similar pattern is also seen for increased LSW thickness (42 yr included in the composite), but in this case the NAC is also strengthened by up to 2.5 Sv.

3) EXPLAINING THE SUBPOLAR GYRE STRENGTH

We have shown that the Nordic seas overflow, the thickness of LSW layer, and the EAP are all significantly correlated with the SPG strength through the 600-yr simulation (Table 3). The correlations between the former three time series are significant, but low. Therefore, we combine these components using a multiple linear regression (Fig. 13) to quantify how much they potentially can explain of the decadal variability in the SPG strength. In the multiple linear regression, the

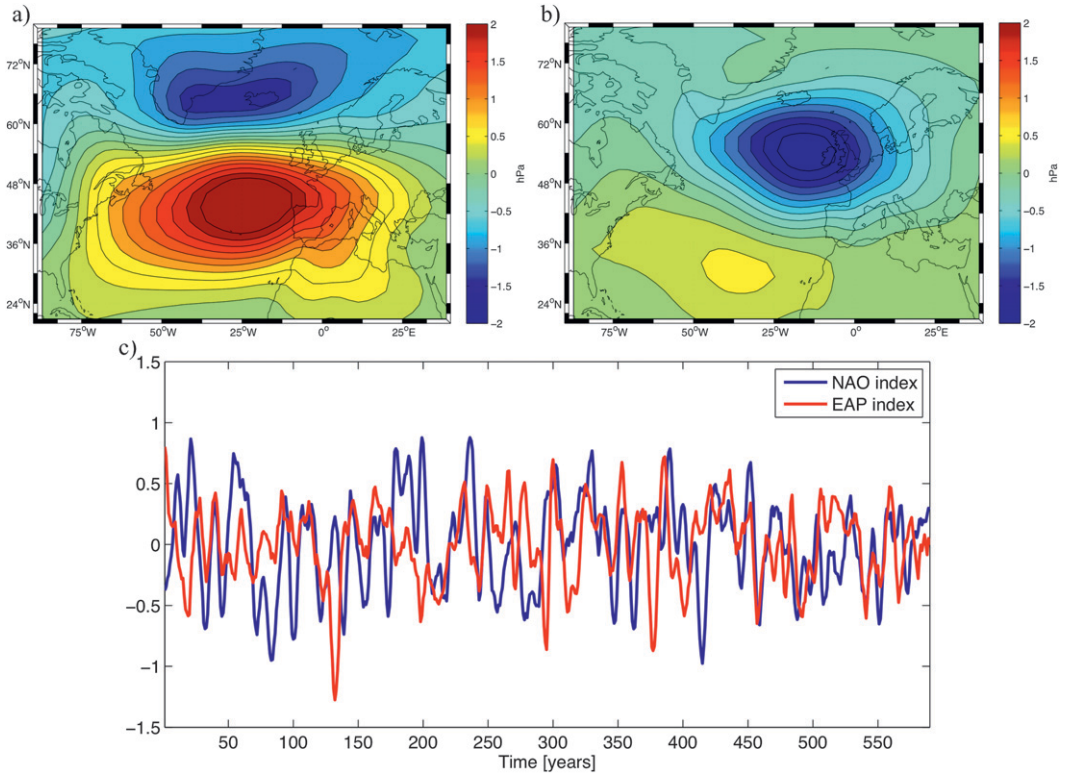

FIG. 11. The (a) first and (b) second EOFs explain 43% and 15%, respectively, of the variance in the winter (Nov–Apr) mean sea level pressure field for the North Atlantic sector. (c) The corresponding first and second principal components, the NAO index, and the EAP index.

time series of the predictors are shifted in time according to the time lags given in Table 3. By comparing the black and red curves in Fig. 13, it is evident that the regression model fits quite well in several periods (e.g., around years 200 and 500) but not in all (e.g., around years 50 and 425). Overall, the SPG strength anomaly is significantly correlated with that of the regression model ($r = 0.66$; i.e., the regression model can explain 44% of

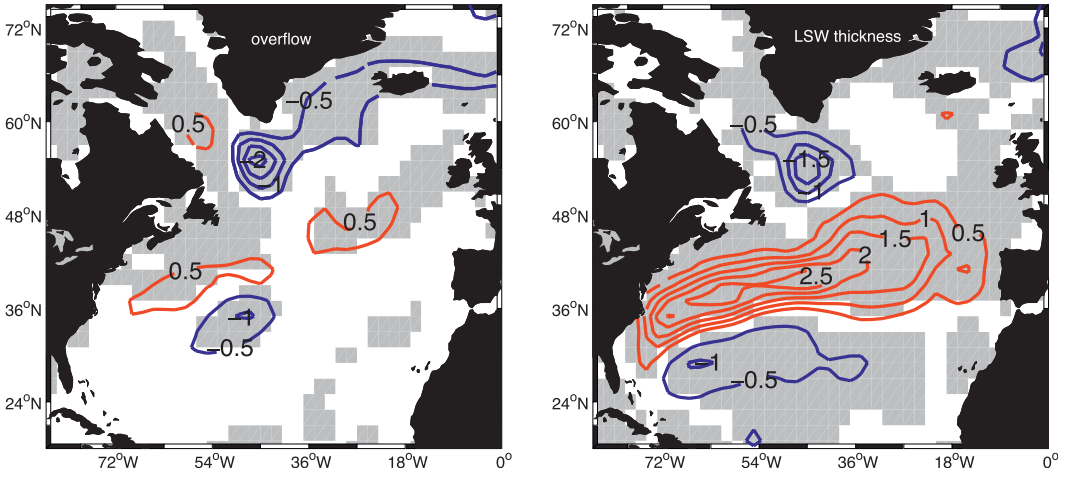

FIG. 12. Composites of anomalies in the barotropic streamfunction for (left) overflow and (right) Labrador Sea Water thickness larger than 1.5 std dev of the filtered time series. Contours are shown with 0.5-Sv intervals. Negative values (blue) imply a strengthening of the cyclonic circulation in the subpolar region. Gray shading indicates significance.

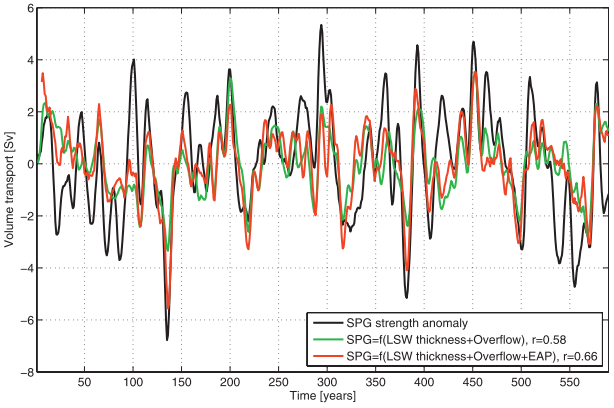

FIG. 13. Anomalous SPG strength modeled using a multiple linear regression as a function of the LSW thickness, the total overflow across the Greenland–Scotland Ridge and the EAP index. The correlation (r) between the modeled SPG strength and the SPG strength derived from the Bergen Climate Model is given in the legend.

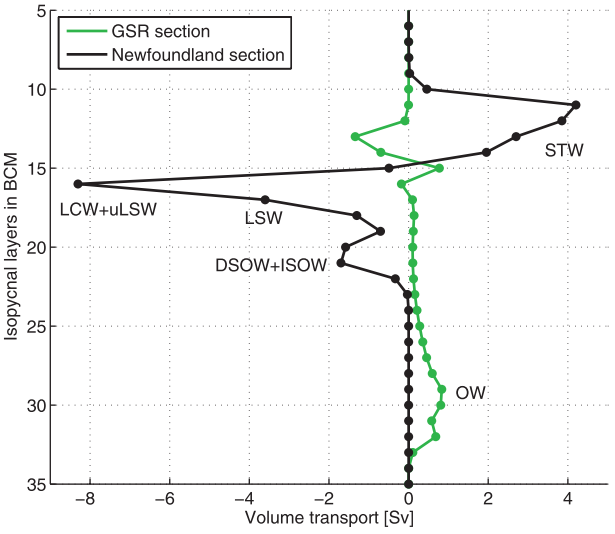

FIG. 14. The net flow across the GSR and through the Newfoundland section in density space (represented by the isopycnal layers in the BCM) is illustrated by the green and black curves, respectively. Positive volume transport denotes net flow into the subpolar region. The mixed layer transports are not included here. Abbreviations are given in Table 1, except for Labrador Current Water (LCW) and upper Labrador Sea Water (uLSW).

the decadal variability). This shows that the changes in the overflow, the LSW thickness, and the EAP index reproduce the decadal variability in the SPG strength relatively well. However, in some periods there are other factors contributing to the variability in the SPG strength. Additional mechanisms, such as the freshwater fluxes associated with the EGC and the southward flow in the Davis Strait, which is not too well simulated in BCM, could also affect the structure of the water column in the Labrador Sea, and hence influence the SPG variability.

4. Discussion

In the previous section we described the main inflows and outflows of the subpolar region in the BCM. The net flow through the GSR and Newfoundland sections are shown in Fig. 14. In the latter there is a large southward transport (8 Sv) in layer 16. About half of this transport is the model representation of the Labrador Current, similarly to the observational estimate of 6.5 Sv (Dengler et al. 2006). The uLSW constitutes the rest of this transport. The STW and OW (Figs. 4 and 6) represent the main water masses flowing into the subpolar region. While circulating in the SPG, these water masses transform. Part of the STW becomes the denser uLSW and LSW as it gradually cools and mixes with fresh Arctic-derived water. The OW becomes the lighter components, DSOW and ISOW, as it cascades down the GSR and mixes with the warm and saline Atlantic-derived water. The rest of the STW continues into the Nordic seas. In the model the processes that govern the transformation are operating on subgrid scales and, hence, the parameterization of these processes is important for the formation and southward progression of the deep water masses (Legg et al. 2009). A larger entrainment of ambient water into the overflow in the Faroe–Shetland Channel would result in a lighter component downstream. This would increase the possibility for the ISOW to escape through the CGFZ and thereby contribute to the DWBC in the western North Atlantic basin.

The southward transport of LSW and DSOW (8.8 Sv) in BCM is less than the observational estimate of the DWBC (12.9 Sv; Schott et al. 2004). This is likely due to the pathway of ISOW, which is mainly located on the eastern flank of the Mid-Atlantic Ridge. If the deep water masses on both sides of the ridge are included, the southward flow of deep water becomes comparable to the observed DWBC. Chlorofluorocarbon (CFC) inventories indicate that some of the ISOW flows through the CGFZ into the western North Atlantic basin, but some also continues southward along the eastern flank of the Mid-Atlantic Ridge (Smethie and Fine 2001).

We have shown that 44% of the decadal-scale variability of the SPG strength can be explained by changes in the overflow, LSW thickness, and the EAP. The decadal-scale variability of the overflow and the LSW thickness also reflect the atmospheric contributions to the circulation. The overflow is related to the Scandinavian Pattern (Bueh and Nakamura 2007; Medhaug et al. 2012), the third mode of North Atlantic sea level pressure variability. During a negative phase of the Scandinavian

Pattern, the northerly winds over the Nordic seas increase, resulting in an increased overflow. This mechanism is described in more detail in Medhaug et al. (2012). In this study the LSW thickness is related to the NAO, which has also been reported in previous studies (Eden and Jung 2001; Bentsen et al. 2004; Bailey et al. 2005).

To further investigate the oceanic response to high NAO+ forcing, the changes in hydrography and the barotropic streamfunction 3 yr after high NAO+ periods have been calculated (Fig. 15). By this 3-yr time lag, anomalies of LSW thickness have propagated from the Labrador Sea to the Newfoundland section. This composite therefore shows the delayed oceanic response as opposed to the composite based on large anomalies of the LSW thickness in the Labrador Sea (Fig. 12). The anomalies in the barotropic streamfunction indicate a northward shift in the NAC, and positive temperature and salinity anomalies are found along the intensified path (Fig. 15). This oceanic response to high NAO+ forcing is similar to what is found in observational, in ocean-only, and in fully coupled model studies (Curry and McCartney 2001; Cooper and Gordon 2002; Lohmann et al. 2009). Lohmann et al. (2009) investigated the response of the SPG to persistent NAO+ forcing. They found that increased LSW formation led to increased advection of STW to the subpolar region, which subsequently led to a decline in the SPG strength. A similar mechanism appears to be operating in the model simulation reported here.

To further understand the influence of the SPG on the neighboring seas, it is also important to investigate the shape of the SPG. For instance, Hátún et al. (2005) found that the hydrography of the Atlantic inflow to the Nordic seas reflects changes in the horizontal extent of the SPG. However, in this model, an increased SPG strength is only associated with a local strengthening confined to the western part of the subpolar basin (Fig. 16, left). In several studies the SPG strength has been constructed using the sea surface height (SSH) in the subpolar region (Häkkinen and Rhines 2004; Hátún et al. 2005). If we, for the model, perform the same analysis using an averaged SSH index in the region 53°–59°N and 41–47°W, we also get a strengthening of the cyclonic circulation in the eastern part of the basin (Fig. 16, right). This indicates more widespread spatial changes associated with SSH variability. This illustrates that even though the SPG strength and the SSH index have a high correlation (Table 3b), these two variables cannot be used interchangeably because of the different response to, for example, atmospheric forcing (the SSH index has a significant correlation with the NAO, while this is not the case for the SPG strength).

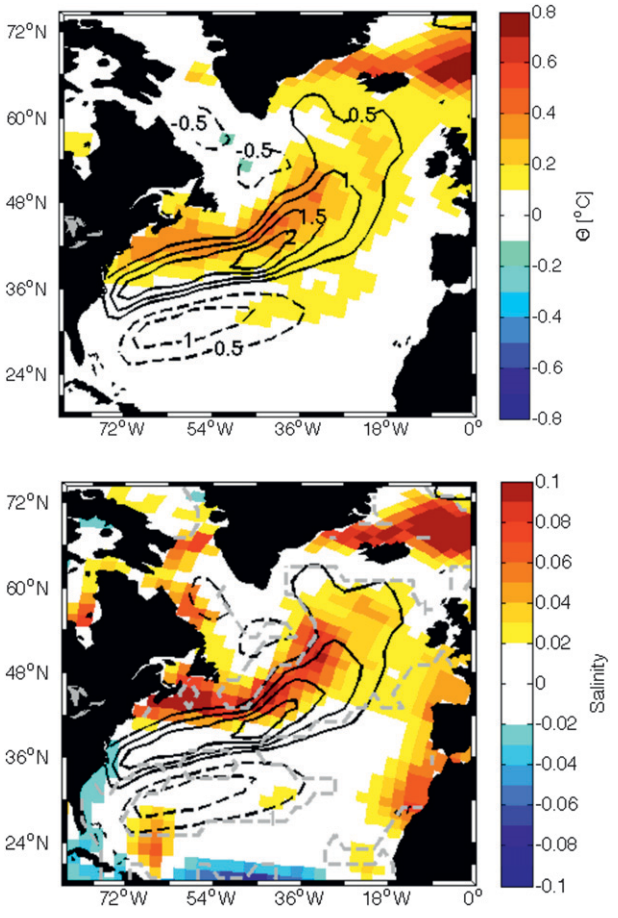

FIG. 15. Composites of anomalies in the barotropic streamfunction (black contours) and mixed layer (top) potential temperature and (bottom) salinity 3 yr after NAO+ periods larger than 1.5 std dev of the filtered time series. Black contours are shown with 0.5-Sv intervals. Negative values (dashed) imply a strengthening of the cyclonic circulation in the subpolar region. Significant values are found within the gray dashed curve (i.e., values above 1).

5. Summary and conclusions

In previous studies, decadal changes in the subpolar gyre (SPG) circulation have been associated with changes in the intensity of deep convection in the Labrador Sea, the strength of the Nordic seas overflow, and upper-ocean hydrography in the northeastern Atlantic (Born et al. 2009; Sarafanov et al. 2010). The goal of this study is to further elucidate these relationships on a decadal scale, using a preindustrial multicentury simulation of the Bergen Climate Model (BCM). Before investigating the decadal variability, the model performance in the subpolar region was assessed with a focus on the model representation of temperature and salinity. These properties of the ocean are key to provide reliable simulations of climate (Bailey et al. 2005). The mean water mass exchanges across the Greenland–Scotland Ridge are well

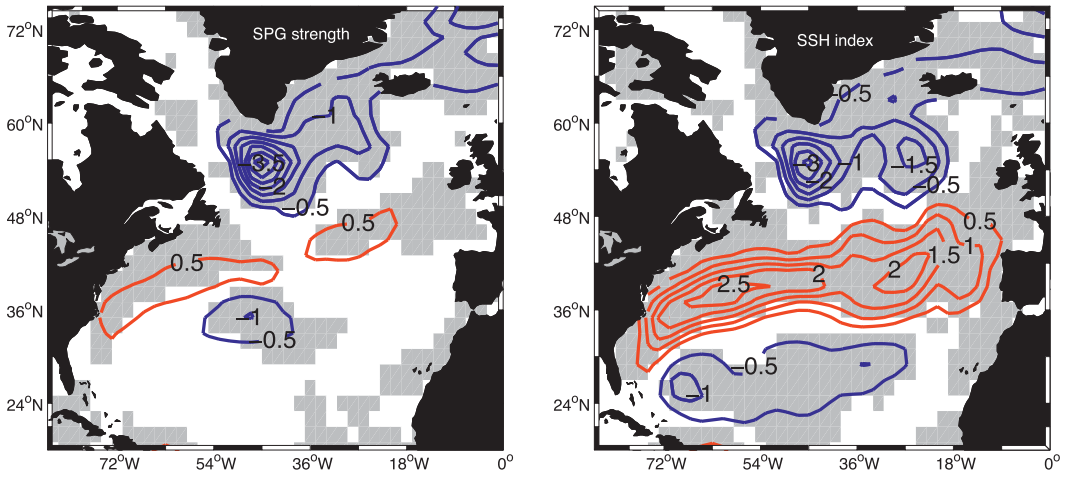

FIG. 16. Composites of anomalies in the barotropic streamfunction for (left) SPG strength and (right) SSH index larger than 1.5 std dev of the filtered time series. Contours are shown with 0.5-Sv intervals. Negative values (blue) imply a strengthening of the cyclonic circulation in the subpolar region. Gray shading indicates significance.

represented in the BCM. In a section stretching from Newfoundland to Portugal the spatial structure of the model hydrography generally compares well with observations. However, the deep western boundary current is less than what is found in observational estimates. This could be due to the Iceland–Scotland overflow water mainly flowing southward on the eastern flank of the Mid-Atlantic Ridge.

In BCM the decadal variability of the Labrador Sea Water (LSW), the Nordic seas overflow, and the East Atlantic Pattern (EAP) are all significantly correlated with the SPG strength. The variability of LSW thickness is partly controlled by the fluctuations of the North Atlantic Oscillation, which are strongly related to the heat flux over the Labrador Sea. The fluctuations of the EAP, on the other hand, are strongly related to the wind stress in the subpolar region. Combining the LSW thickness, the overflow, and the EAP in a multiple linear regression model, these components together can explain 44% of the decadal-scale variability of the SPG strength. The overflow and the LSW thickness have different imprints on the shape of the SPG circulation, where a strengthening of the overflow leads to a localized intensification in the central SPG, while a thickening of the LSW layer is in addition related to the strength of the North Atlantic Current.

There is increasing evidence that the SPG holds a key role in modulating the Atlantic meridional overturning circulation and the exchanges between the Atlantic proper and the Arctic Mediterranean (Hátún et al. 2005; Häkkinen and Rhines 2009; Lohmann et al. 2009; Lozier 2010). It is thus essential to understand the processes affecting the gyre's role in ocean circulation and northern climate. The natural variability of this region must be constrained if the emerging field of climate prediction is to be skillful for the North Atlantic region (Cane 2010; Dunstone and Smith 2010). A continued evaluation of the performance and nature of climate models will allow us to identify which mechanisms are (or are not) robust.

Acknowledgments. This study has been supported by the Research Council of Norway through the BIAC (HRL and TE) and NorClim (IM and OHO) projects. The study has also received funding from the EU FP7 (2007-2013) project THOR under Grant Agreement GA212643 (HRL, TE, and OHO), and the DecCen project (OHO) financed by the Research Council of Norway. We thank Helge Drange, Peter B. Rhines, and Mats Bentsen for insightful and helpful comments when preparing this paper, and three anonymous reviewers for thoughtful and constructive comments. Thanks to Jan Even Ø. Nilsen for helping us with the NISE data, which were provided by the Marine Research Institute, Iceland; the Institute of Marine Research, Norway; the Faroese Fisheries Laboratory; the Arctic and Antarctic Research Institute, Russia; and the Geophysical Institute, University of Bergen, Norway, through the NISE project.

REFERENCES

Aagaard, K., and E. C. Carmack, 1989: The role of sea ice and other fresh water in the Arctic circulation. *J. Geophys. Res.,* **94** (C10), 14 485–14 498.

Bacon, S., 1997: Circulation and fluxes in the North Atlantic between Greenland and Ireland. *J. Phys. Oceanogr.,* **27,** 1420–1435.

——, and P. M. Saunders, 2010: The Deep Western Boundary Current at Cape Farewell: Results from a moored current meter array. *J. Phys. Oceanogr.,* **40,** 815–829.

Bailey, D. A., P. B. Rhines, and S. Häkkinen, 2005: Formation and pathways of North Atlantic Deep Water in a coupled ice–ocean model of the Arctic–North Atlantic Oceans. *Climate Dyn.,* **25,** 497–516.

Barnston, A. G., and R. E. Livezey, 1987: Classification, seasonality and persistence of low-frequency atmospheric circulation patterns. *Mon. Wea. Rev.,* **115,** 1083–1126.

Bentsen, M., H. Drange, T. Furevik, and T. Zhou, 2004: Simulated variability of the Atlantic meridional overturning circulation. *Climate Dyn.,* **22,** 701–720.

Bleck, R., C. Rooth, D. Hu, and L. T. Smith, 1992: Salinity-driven thermocline transients in a wind- and thermohaline-forced isopycnic coordinate model of the North Atlantic. *J. Phys. Oceanogr.,* **22,** 1486–1505.

Böning, C. W., F. O. Bryan, W. R. Holland, and R. Döscher, 1996: Deep-water formation and meridional overturning in a high-resolution model of the North Atlantic. *J. Phys. Oceanogr.,* **26,** 1142–1164.

——, M. Scheinert, J. Dengg, A. Biastoch, and A. Funk, 2006: Decadal variability of subpolar gyre transport and its reverberation in the North Atlantic overturning. *Geophys. Res. Lett.,* **33,** L21S01, doi:10.1029/2006GL026906.

Born, A., A. Levermann, and J. Mignot, 2009: Sensitivity of the Atlantic circulation to a hydraulic overflow parameterization in a coarse resolution model. *Ocean Modell.,* **27,** 132–140.

Brauch, J. P., and R. Gerdes, 2005: Response of the northern North Atlantic and Arctic Oceans to a sudden change of the North Atlantic Oscillation. *J. Geophys. Res.,* **110,** C11018, doi:10.1029/2004JC002436.

Bueh, C., and H. Nakamura, 2007: Scandinavian pattern and its climatic impacts. *Quart. J. Roy. Meteor. Soc.,* **113,** 2117–2131.

Cane, M. A., 2010: Climate science: Decadal predictions in demand. *Nat. Geosci.,* **3,** 231–232.

Cenedese, C., and C. Adduce, 2010: A new parameterization for entrainment in overflows. *J. Phys. Oceanogr.,* **40,** 1835–1850.

Chelton, D. B., 1983: Effects of sampling errors in statistical estimation. *Deep-Sea Res.,* **30,** 1083–1101.

Clarke, R. A., 1984: Transport through the Cape Farewell–Flemish Cap section. *Rapp. P.-V. Reun.- Cons. Int. Explor. Mer,* **185,** 120–130.

Cooper, C., and C. Gordon, 2002: North Atlantic oceanic decadal variability in the Hadley Centre coupled model. *J. Climate,* **15,** 45–72.

Curry, B., C. M. Lee, and B. Petrie, 2011: Volume, freshwater, and heat fluxes through Davis Strait, 2004–05. *J. Phys. Oceanogr.,* **41,** 429–436.

Curry, R. G., and M. S. McCartney, 2001: Ocean gyre circulation changes associated with the North Atlantic Oscillation. *J. Phys. Oceanogr.,* **31,** 3374–3400.

——, ——, and T. Joyce, 1998: Oceanic transport of subpolar climate signals to mid-depth subtropical waters. *Nature,* **391,** 575–577.

de Jong, F., S. S. Drijfhout, W. Hazeleger, H. M. van Aken, and C. A. Severijns, 2009: Simulations of hydrographic properties in the northwestern North Atlantic Ocean in coupled climate models. *J. Climate,* **22,** 1767–1786.

Delworth, T. L., and M. E. Mann, 2000: Observed and simulated multidecadal variability in the Northern Hemisphere. *Climate Dyn.,* **16,** 661–676.

Dengler, M., J. Fischer, F. A. Schott, and R. Zantopp, 2006: Deep Labrador Current and its variability in 1996–2005. *Geophys. Res. Lett.,* **33,** L21S06, doi:10.1029/2006GL026702.

Déqué, M., C. Dreveton, A. Braun, and D. Cariolle, 1994: The ARPEGE/IFS atmosphere model: A contribution to the French community climate modelling. *Climate Dyn.,* **10,** 249–266.

Deshayes, J., and C. Frankignoul, 2008: Simulated variability of the circulation in the North Atlantic from 1953 to 2003. *J. Climate,* **21,** 4919–4933.

Dickson, R. R., and J. Brown, 1994: The production of North Atlantic Deep Water: Sources, rates and pathways. *J. Geophys. Res.,* **99,** 12 319–12 341.

——, J. R. N. Lazier, J. Meincke, P. B. Rhines, and J. Swift, 1996: Long-term coordinated changes in the convective activity of the North Atlantic. *Prog. Oceanogr.,* **38,** 241–295.

Döscher, R., and R. Redler, 1997: The relative influence of North Atlantic overflow and subpolar deep convection on the thermohaline circulation in an OGCM. *J. Phys. Oceanogr.,* **27,** 1894–1902.

Dunstone, N. J., and D. M. Smith, 2010: Impact of atmosphere and subsurface ocean data on decadal climate prediction. *Geophys. Res. Lett.,* **37,** L02709, doi:10.1029/2009GL041609.

Eden, C., and T. Jung, 2001: North Atlantic interdecadal variability: Oceanic response to the North Atlantic Oscillation (1865–1997). *J. Climate,* **14,** 676–691.

——, and J. Willebrand, 2001: Mechanism of interannual to decadal variability of the North Atlantic Oscillation. *J. Climate,* **14,** 2266–2280.

Eldevik, T., J. E. Ø. Nilsen, D. Iovino, K. A. Olsson, A. B. Sandø, and H. Drange, 2009: Observed sources and variability of Nordic seas overflow. *Nat. Geosci.,* **2,** 406–410.

Furevik, T., M. Bentsen, H. Drange, I. K. T. Kindem, N. G. Kvamstø, and A. Sorteberg, 2003: Description and validation of the Bergen Climate Model: ARPEGE coupled with MICOM. *Climate Dyn.,* **21,** 27–51.

Gao, Y. Q., and L. Yu, 2008: Subpolar gyre index and the North Atlantic meridional overturning circulation in a coupled climate model. *Atmos. Oceanic Sci. Lett.,* **1,** 29–32.

Häkkinen, S., and P. B. Rhines, 2004: Decline of subpolar North Atlantic circulation during the 1990s. *Science,* **304,** 555–559.

——, and ——, 2009: Shifting surface currents in the northern North Atlantic Ocean. *J. Geophys. Res.,* **114,** C04005, doi:10.1029/2008JC004883.

Hátún, H., A. B. Sandø, H. Drange, B. Hansen, and H. Valdimarsson, 2005: Influence of the Atlantic subpolar gyre on the thermohaline circulation. *Science,* **309,** 1841–1844.

——, C. C. Eriksen, and P. B. Rhines, 2007: Buoyant eddies entering the Labrador Sea observed with gliders and altimetry. *J. Phys. Oceanogr.,* **37,** 2838–2854.

Holliday, N. P., J. J. Waniek, R. Davidson, D. Wilson, L. Brown, R. Sanders, R. T. Pollard, and J. T. Allen, 2006: Large-scale physical controls on phytoplankton growth in the Irminger Sea. Part I: Hydrographic zones, mixing and stratification. *J. Mar. Syst.,* **59,** 201–218.

Hurrell, J. W., 1995: Decadal trends in the North Atlantic Oscillation: Regional temperatures and precipitation. *Science,* **269,** 676–679.

Kalnay, E., and Coauthors, 1996: The NCEP/NCAR 40-Year Reanalysis Project. *Bull. Amer. Meteor. Soc.,* **77,** 437–471.

Köhl, A., R. H. Käse, D. Stammer, and N. Serra, 2007: Causes of changes in the Denmark Strait overflow. *J. Phys. Oceanogr.,* **37,** 1678–1696.

Kuhlbrodt, T., A. Griesel, M. Montoya, A. Levermann, M. Hofmann, and S. Rahmstorf, 2007: On the driving processes of the

Atlantic meridional overturning circulation. *Rev. Geophys.,* **45,** RG2001, doi:10.1029/2004RG00166.

Lauderdale, J. M., S. Bacon, A. C. Naveira Garabato, and N. P. Holliday, 2008: Intensified turbulent mixing in the boundary current system of southern Greenland. *Geophys. Res. Lett.,* **35,** L04611, doi:10.1029/2007GL032785.

Lazier, J., R. Hendry, A. Clarke, I. Yashayaev, and P. Rhines, 2002: Convection and restratification in the Labrador Sea, 1990–2000. *Deep-Sea Res. I,* **49,** 1819–1835.

LeBel, D. A., and Coauthors, 2008: The formation rate of North Atlantic Deep Water and Eighteen Degree Water calculated from CFC-11 inventories observed during WOCE. *Deep-Sea Res. I,* **55,** 891–910.

Legg, S., and Coauthors, 2009: Improving oceanic overflow representation in climate models: The Gravity Current Entrainment Climate Process Team. *Bull. Amer. Meteor. Soc.,* **90,** 657–670.

Lohmann, K., H. Drange, and M. Bentsen, 2009: Response of the North Atlantic subpolar gyre to persistent North Atlantic Oscillation like forcing. *Climate Dyn.,* **32,** 273–285.

Lozier, M. S., 2010: Deconstructing the conveyor belt. *Science,* **328,** 1507–1511.

Lumpkin, R., and K. Speer, 2003: Large-scale vertical and horizontal circulation in the North Atlantic Ocean. *J. Phys. Oceanogr.,* **33,** 1902–1920.

Marshall, J., and F. Schott, 1999: Open-ocean convection: Observations, theory and models. *Rev. Geophys.,* **37,** 1–64.

Mauritzen, C., 1996: Production of dense overflow waters feeding the North Atlantic across the Greenland–Scotland Ridge. Part 1: Evidence for a revised circulation scheme. *Deep-Sea Res. I,* **43,** 769–806.

McCartney, M. S., and L. D. Talley, 1982: The Subpolar Mode Water of the North Atlantic. *J. Phys. Oceanogr.,* **12,** 1169–1188.

McDougall, T. J., and W. K. Dewar, 1998: Vertical mixing and cabbeling in layered models. *J. Phys. Oceanogr.,* **28,** 1458–1480.

Medhaug, I., H. R. Langehaug, T. Eldevik, T. Furevik, and M. Bentsen, 2012: Mechanisms for decadal scale variability in a simulated Atlantic meridional overturning circulation. *Climate Dyn.,* doi:10.1007/s00382-011-1124-z, in press.

Moore, G. W. K., and I. A. Renfrew, 2005: Tip jets and barrier winds: A QuikSCAT climatology of high wind speed events around Greenland. *J. Climate,* **18,** 3713–3725.

Nilsen, J. E. Ø., H. Hátún, K. A. Mork, and H. Valdimarsson, 2008: The NISE Data Set. Tech. Rep. 08-01, Faroese Fisheries Laboratory, Tórshavn, Faroe Islands, 17 pp.

Nilsson, J., G. Bjork, B. Rudels, P. Winsor, and D. Torres, 2008: Liquid freshwater transport and Polar Surface Water characteristics in the East Greenland Current during the AO-02 Oden expedition. *Prog. Oceanogr.,* **78,** 45–57.

Olsen, S. M., B. Hansen, D. Quadfasel, and S. Østerhus, 2008: Observed and modeled stability of overflow across the Greenland–Scotland ridge. *Nature,* **455,** 519–522.

Orre, S., J. N. Smith, V. Alfimov, and M. Bentsen, 2010: Simulating transport of ^{129}I and idealized tracers in the northern North Atlantic Ocean. *Environ. Fluid Mech.,* **10,** 213–233.

Østerhus, S., W. R. Turrell, S. Jónsson, and B. Hansen, 2005: Measured volume, heat, and salt fluxes from the Atlantic to the Arctic Mediterranean. *Geophys. Res. Lett.,* **32,** L07603, doi:10.1029/2004GL022188.

Otterå, O. H., M. Bentsen, I. Bethke, and N. G. Kvamstø, 2009: Simulated pre-industrial climate in Bergen Climate Model (version 2): Model description and large-scale circulation features. *Geosci. Mod. Dev.,* **2,** 197–212.

——, ——, H. Drange, and L. Suo, 2010: External forcing as a metronome for Atlantic multidecadal variability. *Nat. Geosci.,* **3,** 688–694.

Pèrez-Brunius, P., T. Rossby, and D. R. Watts, 2004: The transformation of the warm waters of the North Atlantic from a streamfunction perspective. *J. Phys. Oceanogr.,* **34,** 2238–2256.

Pickart, R. S., M. A. Spall, M. H. Ribergaard, G. W. K. Moore, and R. F. Milliff, 2003: Deep convection in the Irminger Sea forced by the Greenland tip jet. *Nature,* **424,** 152–156.

Redler, R., and C. W. Böning, 1997: Effect of the overflows on the circulation in the subpolar North Atlantic: A regional model study. *J. Geophys. Res.,* **102** (C8), 18 529–18 552.

Roberts, M. J., and R. A. Wood, 1997: Topography sensitivity studies with a Bryan–Cox-type ocean model. *J. Phys. Oceanogr.,* **27,** 823–836.

Rudels, B., H. J. Friedrich, and D. Quadfasel, 1999: The Arctic Circumpolar Boundary Current. *Deep-Sea Res. II,* **46,** 1023–1062.

Salas-Mélia, D., 2002: A global coupled sea ice–ocean model. *Ocean Modell.,* **4,** 137–172.

Sarafanov, A., 2009: On the effect of the North Atlantic oscillation on temperature and salinity of the subpolar North Atlantic intermediate and deep waters. *ICES J. Mar. Sci.,* **66,** 1448–1454.

——, A. Falina, P. Lherminier, H. Mercier, A. Sokov, and C. Gourcuff, 2010: Assessing decadal changes in the Deep Western Boundary Current absolute transport southeast of Cape Farewell, Greenland, from hydrography and altimetry. *J. Geophys. Res.,* **115,** C11003, doi:10.1029/2009JC005811.

Schlitzer, R., 2000: Electronic atlas of WOCE hydrographic and tracer data now available. *Eos, Trans. Amer. Geophys. Union,* **81,** 45.

Schott, F., and P. Brandt, 2007: Circulation and deep water export of the subpolar North Atlantic during the 1990s. *Ocean Circulation: Mechanisms and Impacts, Geophys. Monogr.,* Vol. 173, Amer. Geophys. Union, 91–118.

——, L. Stramma, and J. Fischer, 1999: Interaction of the North Atlantic Current with the deep Charlie-Gibbs Fracture Zone throughflow. *Geophys. Res. Lett.,* **26,** 369–372.

——, R. Zantopp, L. Stramma, M. Dengler, J. Fischer, and M. Wibaux, 2004: Circulation and deep-water export at the western exit of the subpolar North Atlantic. *J. Phys. Oceanogr.,* **34,** 817–843.

Smethie, W. M., and R. A. Fine, 2001: Rates of North Atlantic Deep Water formation calculated from chlorofluorocarbon inventories. *Deep-Sea Res. I,* **48,** 189–215.

——, ——, A. Putzka, and E. P. Jones, 2000: Tracing the flow of North Atlantic Deep Water using chlorofluorocarbons. *J. Geophys. Res.,* **105,** 14 297–14 323.

Sproson, D. A. J., I. A. Renfrew, and K. J. Heywood, 2010: A parameterization of Greenland's tip jets suitable for ocean or coupled climate models. *J. Geophys. Res.,* **115,** C08022, doi:10.1029/2009JC006002.

Steele, M., R. Morley, and W. Ermold, 2001: PHC: A global ocean hydrography with high-quality Arctic Ocean. *J. Climate,* **14,** 2079–2087.

Stouffer, R. J., A. J. Weaver, and M. Eby, 2004: A method for obtaining initial conditions for use in climate change studies. *Climate Dyn.,* **23,** 327–339.

Sutherland, D. A., and R. S. Pickart, 2008: The East Greenland Coastal Current: Structure, variability, and forcing. *Prog. Oceanogr.,* **78,** 58–77.

Talley, L. D., and M. S. McCartney, 1982: Distribution and circulation of Labrador Sea Water. *J. Phys. Oceanogr.,* **12,** 1189–1205.

Tang, C. C. L., C. K. Ross, T. Yao, B. Petrie, B. M. DeTracey, and E. Dunlap, 2004: The circulation, water masses and sea-ice of Baffin Bay. *Prog. Oceanogr.,* **63,** 183–228.

Thompson, D. W. J., and J. M. Wallace, 2001: Regional climate impacts of the Northern Hemisphere Annular Mode. *Science,* **293,** 85–89.

Tréguier, A. M., S. Theetten, E. Chassignet, T. Penduff, R. Smith, L. Talley, J. Beismann, and C. Böning, 2005: The North Atlantic subpolar gyre in four high-resolution models. *J. Phys. Oceanogr.,* **35,** 757–774.

van Aken, H. M., F. de Jong, and I. Yashayaev, 2011: Decadal and multi-decadal variability of Labrador Sea Water in the north-western North Atlantic Ocean derived from tracer distributions: Heat budget, ventilation, and advection. *Deep-Sea Res. I,* **58,** 505–523.

Wanner, H., S. Brönnimann, C. Casty, D. Gyalistras, J. Luterbacher, C. Schmutz, D. B. Stephenson, and E. Xoplaki, 2001: North Atlantic Oscillation—Concepts and studies. *Surv. Geophys.,* **22,** 321–382.

Yashayaev, I., 2007: Hydrographic changes in the Labrador Sea, 1960–2005. *Prog. Oceanogr.,* **73,** 242–276.

Zhu, J., E. Demirov, F. Dupont, and D. Wright, 2010: Eddy-permitting simulations of the sub-polar North Atlantic: Impact of the model bias on water mass properties and circulation. *Ocean Dyn.,* **60,** 1177–1192.